Open Access
Research Notes

Journal of Agricultural Meteorology 78(2): 78–87, 2022

Methodology to quantify the role of intense precipitation runoff in soil moisture scarcity: a case study in the U.S. South from 1980–2020

Robert Kennedy Smith[a,†], José A. Guijarro[b], Der-Chen Chang[a,c] and Yiming Chen[a]

[a] Department of Mathematics and Statistics, Georgetown University, Washington, D.C. 20057
[b] State Meteorological Agency (AEMET), Balearic Islands Office, Palma de Mallorca, Spain
[c] Graduate Institution of Business Admissions, College of Management, Fu Jen Catholic University, New Taipei City Taiwan

Abstract

The northern U.S. Gulf Coast is among the wettest regions in the contiguous United States, with a transition zone from humid to semi-arid climates occurring between the western Gulf Coast and the 100th meridian. As anthropogenic warming induces more frequent extreme wetting events of greater magnitude, a larger proportion of rainfall runs off unsaturated soils rather than being absorbed and replenishing vegetative water supply. This study introduced novel methodology reliant on reconstructed hourly precipitation intensity data from locations with comprehensive records from the past four decades, incorporating these records into a recursive algorithm measuring daily soil moisture levels. To account for runoff, curtailment multipliers for three different soil classes at each site were applied to 24-hour precipitation totals. Soil moisture balance was then obtained from daily evapotranspiration and infiltrated precipitation, and trends from the autoregressive time series modeling were compared. When runoff quantified by the methodology was considered, average annual soil moisture scarcity trends accelerated for most sample soils, including 13 of the 15 highly-infiltrative soils showing a change relative to the unrestricted infiltration in the reference case. The findings, however, were generally not statistically significant. These results are suggestive, but not conclusive, of a growing role from intense precipitation in drought development for the selected region. The seasonality of evolving rainfall rates in the case study area may explain the limited impact, as intensity rates are growing most quickly during the wintertime, a period when episodes infrequently exceed maximum soil infiltration capacity. The methods introduced here, achieving superior accuracy at precise locations relative to gridded products, are reproducible for global locations with adequate data coverage.

Key words: Evapotranspiration, Precipitation, Runoff, Soil moisture

1. Introduction

The southern region of the United States between the Florida panhandle and the 100th meridian is highly productive, diverse land essential for lumber production, high-value agricultural crops, and pasture (Howard and Liang, 2019; USDA, 2017). It houses two of the five largest U.S. metropolitan areas, Dallas and Houston, with robust demand growth for municipal water (Texas Water Development Board, 2017; McGregor, 2015). New methodology using location-specific observed climate and soil data is applied to this locale to show how recent changes in rainfall intensity rates have altered soil moisture, accounting for episodes that exceed hourly infiltration capacity within a daily algorithm framework.

Analyses of historical data and projections of future conditions in the case study area are in consensus that events during which heavy precipitation falls are increasing in frequency and magnitude (Janssen *et al*., 2014; Melillo *et al*., 2014; Skeeter *et al*., 2019). Globally, the warming climate has intensified the hydrological cycle, with the Clausius Clapeyron relationship estimating a seven-percent increase in average precipitation intensity per degree Celsius of warming from higher specific humidity values (Kharin *et al*., 2007; Mishra *et al*., 2012; Trenberth, 2011). This is supplemented by evolving atmospheric dynamics aggregating convection into heavily precipitating cloud formations (Lackmann, 2013). As convective available potential energy (CAPE) and convective inhibition (CIN) swell in a warmer climate, the frequency of strong convection will grow as weak and moderate organization diminishes (Liu *et al*., 2017). Although the South has experienced a lesser increase in such events than the Northeast (Horton *et al*., 2014), average precipitable water values over the Gulf of Mexico have grown by 7.3 percent between 1980 and 2018 (Wang *et al*., 2018). Enhanced rainfall from tropical cyclones has recently devastated parts of the region, a trend projected to accelerate due to global (Bhatia *et al*., 2019) and local factors (Zhang *et al*., 2018).

Shifts in the total amount of annual precipitation and the temporality of occurrences determine the change in soil moisture levels. The location and intensity of the North Atlantic subtropical high (NASH), colloquially referred to as the Bermuda high, is highly consequential for the region's hydrology. During the summertime when NASH is strongest,

Received; December 27, 2021
Accepted; February 9, 2022
†Corresponding author: rks21383@gmail.com
DOI: 10.2480/agrmet.D-21-00054

a westward shift has caused more variability in interannual warm season precipitation totals (Li *et al*., 2013). By running a June 2010 weather pattern under the high emissions scenario of the Coupled Model Intercomparison Project Phase 5 (CMIP5, RCP8.5) and relating historical rainfall with modeled values, Ferreira *et al*. (2018) found that the intensity and amount of precipitation increased from the atmospheric dynamics of the warmer environment. This enhanced wetting was attributed to greater mesoscale convection, although the authors did not find a correlation between the organization and the intensity at which the rain fell. In agreement with the literature, they found the most robust increases over the Gulf of Mexico and immediate coastal areas (Rasmussen *et al*., 2017). Even though the study covered the Southeast and included the Atlantic Coast, its western half overlapped with the eastern half of this analysis.

During fall, the NASH weakens, but the location of its western ridge remains critical to the conveyer of moisture from the Western Caribbean and Gulf of Mexico into the Southern U.S. Bishop *et al*. (2018) have found a 37-percent increase (87 mm) in fall precipitation in the South (in a study area whose boundaries are similar those examined here). This autumnal wetting accounts for nearly three-quarters of the annual positive precipitation trend (Easterling *et al*., 2017).

Limited hourly precipitation data (Trenberth *et al*., 2017) contrasts with the abundant data available on a daily resolution from gridded sets and direct observation networks. Brown *et al*. (2019, 2020) have authored two studies, finding that cold-season hourly precipitation rates have increased most rapidly from 1960−2017, and approximately half of 50 locations across the U.S. South have shown statistically significant annual intensity increases ($p<0.05$). Using a data homogenization algorithm and a recursive soil moisture algorithm, this study related the previous discussion to vegetative soil water supply and quantified the implications of changing precipitation on agricultural drought through the introduction of new methods. A brief background on the region's climate is provided, followed by a description of the two algorithms deployed in the analysis. The findings are then discussed, providing context for past and future hydrological implications in the geographic area of study.

2. Materials and Methods

2.1 Climate of the region

The case study region (from the 88th meridian in the East to the 100th meridian in the West) was chosen due to its role as a transition zone between humid and semi-arid climates and its absence of mountainous topography affecting infiltration. The region's ubiquitous pine forests and prairies in drier climates can be effective carbon sinks for biosequestration, increasingly attracting private and public-sector interest (Clark *et al*., 2016; Zhu *et al*., 2016). Although the states bordering the Gulf of Mexico lack orographically-induced microclimates, annual rainfall along the Northern Gulf Coast is among the highest in the contiguous U.S., showing a decline away from the shoreline that is most pronounced moving West into Texas. Mobile, Alabama (the easternmost location in this study) receives 1,681 mm of annual precipitation, while San Angelo records less than one-third of that total (538 mm) in an average year (NOAA, 2012).

The semi-arid interior Texas locations are highly vulnerable to severe drought (Nielsen-Gammon *et al*., 2020), while wetter coastal areas are directly impacted by tropical cyclones (Rappaport *et al*., 2010). All locations experience interannual precipitation variability and heavy rainstorms (Brown *et al*., 2020). As anthropogenic warming has augmented reference evapotranspiration and the frequency and severity of extreme rainfall events – trends forecast to accelerate in the future – impacts on soil moisture levels will continue to affect the South's water demand and current ecosystem viability.

2.2 Calculating soil moisture deficits

Daily soil moisture levels at the specific locations (Figure 1 and Table 1) were determined by reference evapotranspiration (ET_0) modeled from the FAO-56 Penman-Monteith (FOA-56 PM) equation (Zontarelli *et al*., 2010). An explanation of station inclusion is found later in this section, but sufficient hourly precipitation data coverage to support the novel methodology was a perquisite. FOA-56 PM parameters were obtained from the National Centers for Environmental Information (NCEI) Global Summary of the Day (GSOD) network, with the exception of solar data interpolated from the North American Regional Reanalysis (NARR) (Mesinger *et al*., 2006) and the bias-corrected North, American Land Data Assimilation System (NLDAS-2) (NASA, 2021), as NCEI does not publish daily shortwave radiation values. NLDAS-2 values are corrected with the University of Maryland Surface Radiation Budget dataset, utilizing GOES-8 satellite data and ratio-based adjustments (Berg *et al*., 2003). The data was available at a 4-km gridded partition resolution (0.04167 deg.). Daily precipitation values originated from NCEI's quality-controlled Global Historical Climatology Network (GHCN). As in previous analyses (Smith *et al*., 2020), the reference vegetative surface covering assumed for ET_0 was fescue grass (Wright, 1993) with an adjustment assigned for cold days during which plant life remained dormant (Jensen and Allen, 2016). The U.S. Department of Agriculture's Web Soil Survey (USDA, 2019) provided the total available water holding capacity of three soil types at each 40,400-hectare (100,000-acre) plot surrounding the observation station in the top one meter of soil, representing the available supply of moisture at maximum grass root depth between saturated conditions and the wilting point. In the absence of rainfall, the fescue was assumed to draw moisture at the rate of ET_0 until 60 percent of the supply remained. A curtailment coefficient of $K_{s,t}$ was then introduced and evapotranspiration was represented as $K_{s,t} * ET_0$ where $t=\{1/1/1979, ..., 31/12/2020\}$. Here $K_{s,t}$ was a proxy for drought, with values at one representing a well-watered state and values of zero occurring at the wilting point, well past the survival rate of most vegetation, which begins suffering irreparable damage near $K_{s,t}$ values of 0.2 (Wright, 1993).

The 1979−2020 daily climate parameters imputed into the FOA-56 PM were homogenized by the *Climatol* algorithm (Guijarro, 2019). For 18 first-order observation sites across the South, GHCN and GSOD data were collected along with data from nine additional stations in closest proximity to each of the locations. The 18 core stations, all located at regional or international airports, are represented in both datasets, however

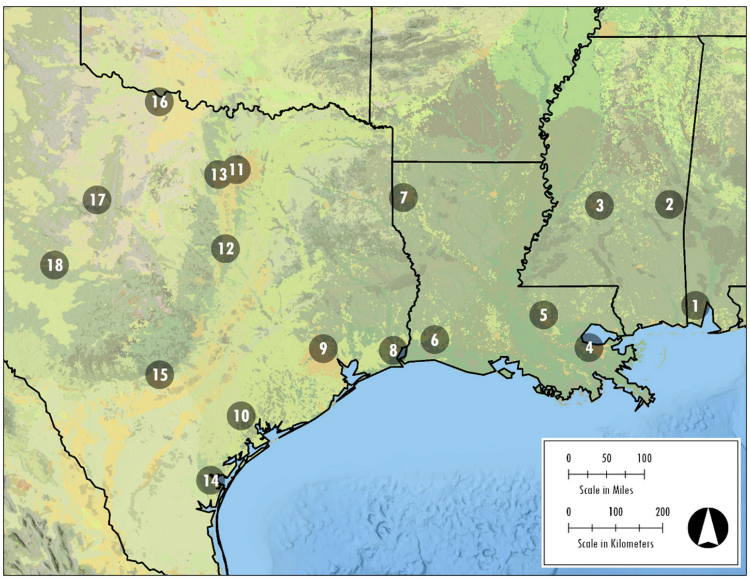

Fig. 1. Observation sites (In all figures, results are displayed from the easternmost location (1) to the westernmost (18)).

Table 1. Observation sites, moving East to West.

Station ID and Name	Lat.	Long.	Station ID and Name	Lat.	Long.
1. Mobile Regional AP, AL	30.69	-88.25	10. Victoria Regional AP, TX	28.86	-96.93
2. Meridian Key Field, MS	32.33	-88.74	11. DFW Int'l AP, TX	32.90	-97.02
3. Jackson Int'l AP, MS	32.32	-90.08	12. Waco Regional AP, TX	31.62	-97.23
4. New Orleans Armstrong Int'l AP, LA	30.00	-90.28	13. FW Meacham Field, TX	32.82	-97.36
5. Baton Rouge Metro AP, LA	30.54	-91.15	14. Corpus Christi Int'l AP, TX	27.77	-97.51
6. Lake Charles Regional AP, LA	30.12	-93.23	15. San Antonio Int'l AP, TX	29.54	-98.48
7. Shreveport Regional AP, LA	32.45	-93.82	16. Wichita Falls Muni. AP, TX	33.98	-98.49
8. Port Arthur/ SE TX Regional AP, TX	29.95	-94.02	17. Abilene Regional AP, TX	32.41	-99.68
9. Houston Intercontn'l Airport, TX	29.98	-95.36	18. San Angelo Mathis Field, TX	31.35	-100.50

the neighboring stations are largely unique to the specific network. These sites were used to infill rare missing records from primary stations. After acquiring each GHCN and GSOD cluster, *Climatol* aggregated daily observational data into monthly series and deployed the Standard Normal Homogeneity Test (SNHT threshold of 25) to determine discontinuities within the aggregate means.

Even within the highest-quality GHCN networks, this homogenization corrected potential equipment observation biases as well as reporting errors. For example, *Climatol* detected a non-first order GHCN cluster station reporting 203.2 mm of precipitation for 17 consecutive days and removed the erroneous observations. More subtle inhomogeneities result from equipment calibration issues, relocations to different areas of the same campus, or nearby physical obstructions such as buildings and natural barriers that partially shield instruments from the elements. After detecting each breakpoint, the affected series was split, disaggregated back into its daily resolution, and reconstructed as multiple series using a distance formula with the normal ratio values of neighboring stations (Smith *et al*., 2020). The resulting daily FOA-56 PM climate parameters for the 18 first-order stations offered complete coverage. Moreover, *Climatol* mitigated the risk of false trends from reporting irregularities as well as sample biases within each cluster (e.g. the inclusion of a "wetter" station whose reporting history covers the latter half of the analyses period).

Monthly total evapotranspiration and precipitation were then calculated. Using the R Project for Statistical Computing and packages "dynlm", "lmtest", "sandwich", and "TSA", the data (and all subsequent sets) were seasonally adjusted and autoregressive (AR) time series modeling was completed, with the order of each model determined by the Akaike information criterion. Trends in soil moisture scarcity, resulting from the temporal balance of evapotranspiration and precipitation, and a representation of agricultural drought, were measured in two ways: the monthly value of $\int 1-K_{s,t}\,dt$ and the hypothetical irrigation water demand to preserve $K_{s,t} > 0.7$, the level at which fescue grass begins to change in appearance from well-watered to moisture-stressed. Hypothetical irrigation demand, interchangeably referred to in this analysis as supplemental water demand, was represented by the introduction of 25.4 mm (one inch) of water in the recursive soil moisture algorithm at each day when $K_{s,t}$ dropped below 0.7. When this criterion was met on rainy days, the amount of supplemental water was reduced by the amount of rain received, unless rainfall exceeded 25.4 mm, in which case no irrigation occurred.

2.3 New methodology representing hourly extreme precipitation runoff in the daily algorithm

Some or all of the above methods have been deployed in prior analyses (e.g. Ficklin *et al*., 2015; Kramer *et al*., 2015, Smith and Chang, 2020) that do not account for water hitting the surface at

a rate that exceeds the infiltration capacity. This runoff, which is ineligible to replenish soil moisture, has become increasingly consequential as the intensity of rainy periods has grown. While the recursive algorithm as described assumed precipitation reaching soils holding their total available water capacity either flowed away or percolated into the water table, all other water was assumed to be absorbed and previously considered eligible to accordingly reduce moisture deficits. To represent the impacts on soil moisture from extreme events and enhance the previously-developed product, USDA's Web Soil Survey (USDA, 2019) was again consulted for saturated hydraulic conductivity (K_{sat}) values. Soils at the 25th, 50th, and 75th K_{sat} percentiles were chosen to represent the range of ideal growing conditions (USDA, 1999), removing heavy clays and sandy ground in most areas. Using the same plots from which water holding capacity originated, three site-specific K_{sat} rates (Table 2) were obtained to acquire $\psi_{k,j}$, the infiltration rate (mm hr^{-1}), where k={1, ..., 18} and j={1, 2, 3} comprise the set of locations and K_{sat} percentiles, respectively.

Before concluding with the inclusion of extreme rainfall into the soil moisture algorithm, a brief note is provided on the number of elements comprising set k: Within the predetermined area of study, candidate sites with 1979–2020 observation records in NCEI's Integrated Surface Database (ISD) network were examined for hourly precipitation coverage. ISD data from the stations was cleaned, sorted, reformatted, and time-shifted to Central Standard Time, and any station with less than 90 percent coverage over the 42-year period was excluded. The number of missing hours per year was aggregated and regressed against time. If a station's coverage showed a statistically significant increase with time (a more likely occurrence than the converse since post-2003 records have fewer omissions), that station was dropped from consideration, as greater use of a relatively distant proxy station in early years would introduce bias. With two exceptions, all stations in the resulting set k had hourly coverage rates exceeding 99 percent. Unlike the isolated missing daily records, where abundant nearby GHCN and somewhat less abundant GSOD stations were used as infill, the scarcity of alternative hourly reporting stations from the first half of the analysis period would result in more accurate proxy locations after 2003. Therefore, the nearest station in set k was selected as the proxy. If that location were also missing the same record, *Climatol* would continue searching for the nearest reporting station. As mentioned, each station k = {1, ..., 18} had corresponding near-complete GHCN and GSOD coverage common to first-order stations. This ensured that the sum of reconstructed hourly ISD precipitation almost always equaled the daily GHCN value for all k, t and that any deviations were slight.

For k={1, ..., 18}, let $P_{h,t,k}$ equal the amount of precipitation falling in hour h on day t where h={1, ..., 24} and t={1/1/1979, ..., 31/12/2020}. The daily curtailment factor, $C_{t,k,j}$, as a function of hourly runoff, $Q_{h,t,k,j}$, where j represents one of three percentile classes in region k is given by the following:

$$(1)\ \forall P_{h,t,k} > \psi_{k,j}\ let\ Q_{h,t,k,j} = P_{h,t,k} - \psi_{k,j},\ and\ \forall P_{h,t,k} \le \psi_{k,j}\ let\ Q_{h,t,k,j} = 0,$$

$$then\ C_{t,k,j} = 1 - \frac{\sum_{h=1}^{24} Q_{h,t,k,j}}{\sum_{h=1}^{24} P_{h,t,k}}$$

$C_{t,k,j}$ was applied to the recorded daily precipitation in the soil moisture algorithm, with $K_{s,t}$ and supplemental water demand trends again measured through seasonally-adjusted AR modeling. The magnitude of the trends in these representations of agricultural drought was compared to those previously quantified without accounting for extreme hourly rainfall runoff.

3. Results

3.1 Increased aridity found under reference assumptions

In agreement with other studies (e.g. Wehner *et al*., 2017; Seager *et al*., 2018), warming temperatures have caused higher reference evapotranspiration rates at 17 of 18 case study locations from 1979 through 2020, with 10 of these trends exhibiting statistical significance (p<0.10). Simultaneously, only seven locations showed positive precipitation trends, and no trend was significant in either direction. The aggregate change in these two parameters is displayed in Figure 2, with the modeled AR 2020 values compared with modeled AR 1979 data. As with all forthcoming figures, the graphed values do not represent historical observations but rather modeled annual normal amounts occurring at the beginning and end of the analysis period derived from time series regressions. Statistical significance in Figures 2 and 4 are denoted with solid bars. For example, Wichita Falls, TX (Station 16) has seen normal annual reference evapotranspiration increase from 1,652 mm in 1979 to 1,826 mm in 2020, with the 174-mm difference shown in Figure 2.

Relating moisture-limited evapotranspiration to rainfall occurrences on a daily temporal resolution produced the seasonally-adjusted monthly integral value and the hypothetical monthly irrigative watering demand to preserve the well-watered grass surface covering. Although the integral value is more precise, results are presented and discussed using the more intuitive assumed supplemental water metric. Figures 3 and

Table 2. 25th, 50th, and 75th percentile steady-state USDA soil infiltration rates (K_{sat}) (mm hr^{-1}).

Stn. / mm hr^{-1}	25th	50th	75th	Stn. / mm hr^{-1}	25th	50th	75th
1. Mobile Reg.	45.0	73.5	93.1	10. Victoria Regional	4.1	5.6	9.2
2. Meridian Key Fld.	7.0	16.4	31.0	11. DFW Int'l	0.9	6.1	54.9
3. Jackson Int'l	23.8	31.5	41.3	12. Waco Regional	3.2	12.2	36.2
4. NOLA Armstr. Int'l	0.9	10.4	23.1	13. FW Meacham Fld.	34.2	64.7	67.5
5. Baton Rouge Metro	12.7	19.3	23.5	14. Corpus Christi Int'l	2.7	2.7	3.9
6. Lake Charles Reg.	3.3	6.3	6.3	15. San Antonio Int'l	2.5	3.3	12.2
7. Shreveport Reg.	11.6	19.8	30.9	16. Wichita Falls Muni.	10.0	17.3	40.5
8. Port Arth/ SE TX Reg	0.9	0.9	1.6	17. Abilene Regional	5.6	17.3	36.9
9. Houston Intcontn'l	12.2	18.0	18.0	18. San Angelo Mathis	22.7	24.6	24.6

4 show the change in hypothetical modeled 2020 aggregate irrigation relative to 1980 in the reference case (without accounting for runoff). Climatological parameters from 1979 were used to calibrate soil moisture levels and so that year was excluded from subsequent regression analyses. Figure 2 is highly correlated with Figures 3 and 4, but differences result from precipitation seasonality: this explains why Fort Worth, TX (Station 13) has the greatest change in supplemental water demand but only the third-highest difference between the net change in expected 1979–2020 annual precipitation and ET_0 values.

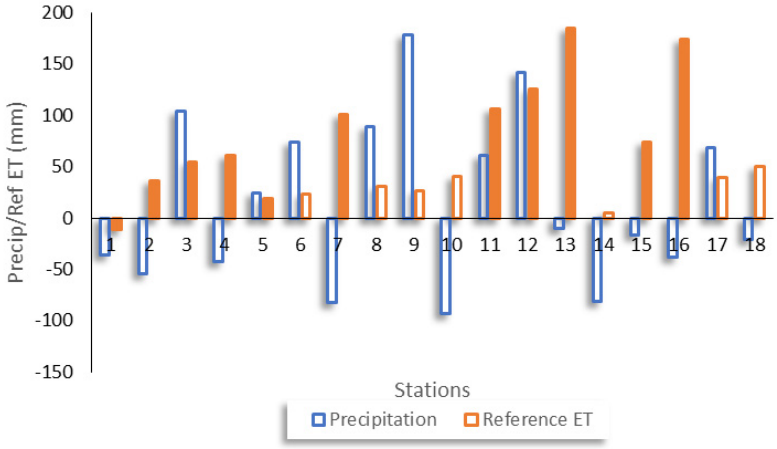

Fig. 2. Modeled AR 2020 average annual reference evapotranspiration and precipitation change, relative to modeled AR 1979 values. Fill denotes statistical significance (mm).

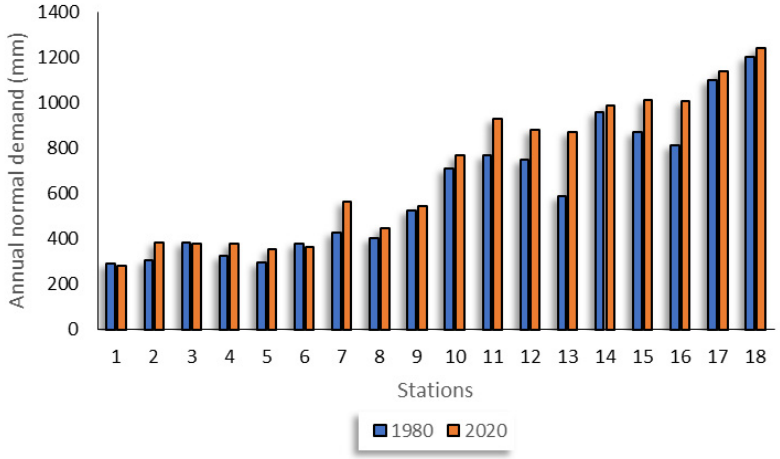

Fig. 3. Modeled AR 2020 average annual hypothetical vegetative water demand, relative to modeled hypothetical 1980 AR values (mm).

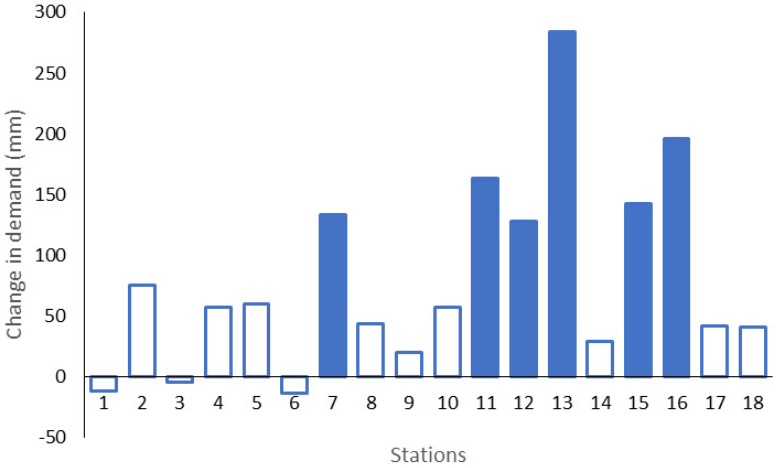

Fig. 4. Modeled AR 2020 change in average annual hypothetical vegetative water demand, relative to hypothetical modeled AR 1980 values. Fill denotes statistical significance (mm).

3.2 Accelerated moisture scarcity trends when considering extreme precipitation

New calculations incorporating runoff from precipitation events that exceeded the location-specific hourly infiltration rates at the three soil classes caused average annual 1980−2020 hypothetical watering demand to grow by varying degrees, as shown in Table 3, with the exception of the easternmost station, where virtually all water was infiltrated into the highly-absorptive ground. The previously unaddressed issue answered in this analysis was whether the documented increases in heavy event frequency and magnitude have accelerated trends in soil moisture scarcity and, if so, to what degree. Under the reference scenario, with water hitting the surface ineligible to satiate vegetative demand only once the total available water capacity was exceeded, there were six statistically significant increases in assumed supplemental water demand out of the 15 positive trends; none of the three negative trends exhibited significance. Under the 25th, 50th, and 75th percentile K_{sat} assumptions, one additional location with a drying trend gained significance (Station 8) and one station with a negative reference case trend flipped to having a positive value (Station 6). These changes were found in all three soil class scenarios. Relative to reference trend values, 11 of the 17 stations whose trends differed for 25th percentile soil classes showed accelerated drying as did 12 of 17 stations when utilizing 50th percentile infiltration data. When applying 75th percentile infiltration rates, Stations 3 and 11 joined Station 1 in having the same time series irrigative water demand trends as their respective reference scenarios, and therefore, only 15 locations had trend variance. Of these, 13 showed soil moisture scarcity developing at a faster rate with time, however the comparisons did not hold statistical significance. The four infiltration rate assumptions for which hypothetical watering demand were modeled are summarized in Figures 5 and 6. Figure 5 graphs 2020 modeled values relative to 1980 for all four scenarios and Figure 6 offers a comparison of the calculated 41-year change when measuring applied station-specific 25th, 50th, and 75th percentile K_{sat} rates against the unrestricted reference.

4. Discussion

4.1 Simplified infiltration assumptions representing real-world conditions

This section is comprised of four topic areas: a discussion of infiltration assumptions, an interpretation of the results, a validation of the methodology that ascertained how runoff is changing soil moisture profiles, and concluding remarks. Deploying K_{sat} to represent infiltration capacity presumed a constant rate that is observed after the wetting front has penetrated into the subsurface, following several hours of precipitation (Rawls *et al*., 1993). As modeled by Green and Ampt (Nearing *et al*., 1996), infiltration in dry soils shows exponential decline, converging to a steady-state horizontal asymptote of $y = K_{sat}$. Use of this parameter for $\psi_{k,j}$ underestimated hourly infiltration capacity, except when heavy rains fell on wet soils or induced absorption-impeding surface crusting (Al-Kaisi, 2012). Vegetative coverings, cultivation practices, and cracking also modify the slopes of infiltration curves and steady-steady rates, resulting in discrepancies between field measurements and the modified laboratory-predicted values from Uhland and O'Neal used in the USDA Web Soil Survey (USDA, 2003). Due to the way hourly curtailment factors were applied to daily parameters in this analysis, the scarcity of available multidecadal subhourly datasets, the assumption that all $P_{h,t,k} \leq \psi_{k,j}$ was fully absorbed before ponding occurred, and the difficulty in estimating and obtaining input values required for Green-Ampt calculations, such as effective suction and soil porosity, assumed $\psi_{k,j}$ values were not time or state dependent. Field tests calculate highly-variable $\psi_{k,j,t}$ values, with the t subscript denoting subhourly intervals, whose values are often non-transferrable to similar plots.

4.2 Interpretation of results by soil classification

Figure 6 is characterized by mixed trends for the 25th percentile soil classes relative to the unrestricted reference, trending toward near-universal accelerated drying for soils with higher K_{sat} rates. The smaller magnitude of change relative to zero at most locations was expected with the higher percentile classes, as there was generally less change relative to the unrestricted reference for soils that absorb a relatively high proportion of intense rainfall. If only the precipitation intensity were changing and not the number of hours during which rainfall was recorded, the region would be getting wetter and the positive correlation between runoff and moisture scarcity as measured with time would be strongest and have the greatest magnitude for the soils with the lowest infiltration rates. The historical data instead showed mixed, statistically insignificant accumulated precipitation trends. More frequent episodes of higher intensity are coinciding with fewer hours of rainfall at

Table 3. Average annual hypothetical irrigative water demand for the unrestricted reference scenario and when accounting for curtailed infiltration rates from 25th, 50th, and 75th percentile soil classes (mm yr^{-1}).

Stn. / mm yr^{-1}	Ref.	25th	50th	75th	Stn. / mm yr^{-1}	Ref.	25th	50th	75th
1	287.7	287.9	287.7	287.7	10	739.8	917.8	868.6	809.6
2	344.5	435.6	362.4	345.2	11	849.2	1260.0	954.4	849.2
3	380.6	385.6	304.8	380.6	12	816.4	1006.2	851.9	817.0
4	352.4	912.6	414.0	359.9	13	732.7	734.4	732.8	732.8
5	326.5	364.9	335.6	330.6	14	974.5	1178.4	1178.4	1133.2
6	374.3	617.3	496.9	496.9	15	943.3	1154.2	1117.0	978.8
7	496.7	535.9	506.8	498.1	16	911.9	954.0	924.4	912.0
8	428.2	956.3	950.0	832.9	17	1120.3	1210.8	1135.7	1121.9
9	535.4	584.0	551.8	551.8	18	1224.0	1231.2	1230.0	1230.0

most locations, although all time series trends measuring the number of precipitation hours with time were also insignificant. Locations with higher rainfall intensities during a lesser number of wetting hours experience a greater amount of runoff whenever rainfall does occur, but fewer overall hourly occurrences. Soils with low K_{sat} values are therefore most affected by the reduction in low and moderate precipitation events. Figure 7 shows average 1979–2020 intensities by station and number of wet

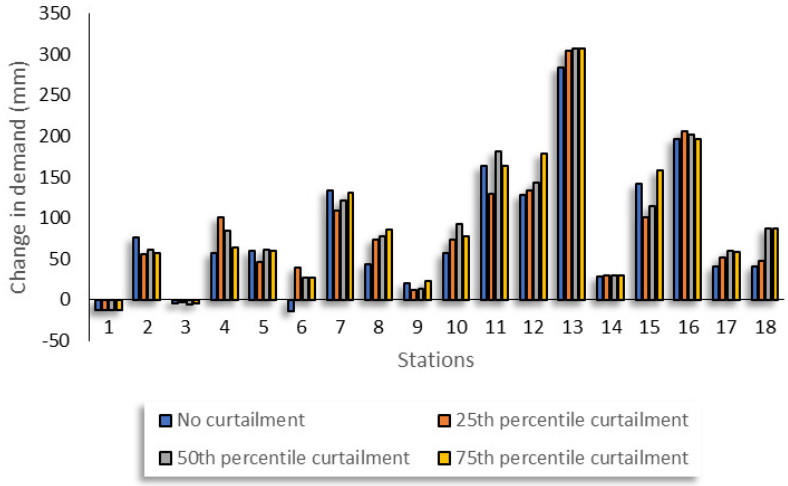

Fig. 5. Comparisons of AR modeled 1980–2020 change in hypothetical irrigative water demand by soil infiltration rate (K_{sat}) percentile (mm).

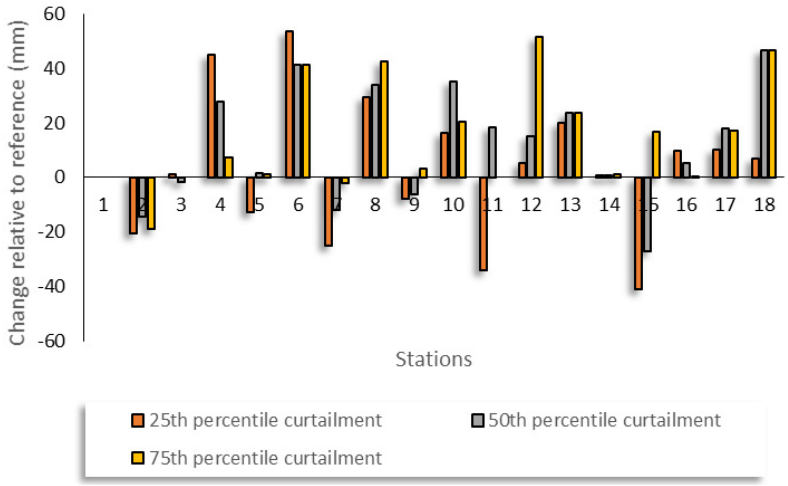

Fig. 6. 25th, 50th, and 75th K_{sat} percentile 1980–2020 change in hypothetical irrigative water demand, relative to reference unrestricted infiltration.

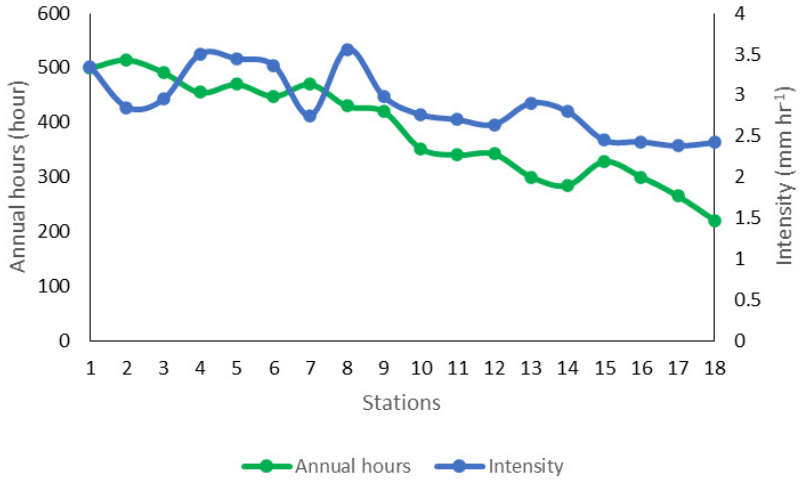

Fig. 7. Moving East to West, the average number of precipitation hours and precipitation intensity (mm hr^{-1}).

hours; moving westward from the humid northern Gulf Coast to the semi-arid Texas plains. Soils comprising the 25th percentile K_{sat} rates – generally clays – absorb less water per hour than the average rainfall intensities at five locations, demonstrating the impact from a lesser number of rainy periods.

For loamy and sandy soils, the seasonality during which precipitation intensification has occurred also limits additional runoff. As Brown *et al*. (2019) found, winter precipitation in the U.S. South is intensifying most rapidly, yet, for the 50th percentile soils in this sample, winter events rarely exceed hourly infiltration capacities. At three sites representing the range of climatological conditions found in the area of study, Mobile, AL, Houston, TX and San Angelo, TX (Stations 1, 9 and 18, respectively), wintertime offered a period of relative dormancy for heavy events. In Mobile, 12.8 percent of 1980–2020 runoff attributable to intense downpours on 50th percentile soils occurred during December, January, and February (DJF). The DJF proportion was found to be lower in Houston and Abilene: 7.4 and 3.2 percent, respectively. Therefore, augmented winter event intensities in this region are less likely to exceed K_{sat} thresholds for the more absorptive soils. While soil moisture in the South is generally lowest in August, September, and October, it is at its zenith in January, February, and March (NWS, 2021). Daily algorithms that disallow moisture falling on saturated soils, such as the reference case of the recursive algorithm deployed here, already tabulate most winter runoff. Although cold-season flood risk is diminished with respect to hourly infiltration excesses, more intense winter events leave the South highly vulnerable to flooding from precipitation falling on saturated ground (Lecce, 2000).

4.3 Validation of methods with observation records

Even though this new approach deployed quality-controlled, homogenized observational parameters, the simplified models that represented vegetative moisture supply and precipitation runoff require validation. Calculated reference evapotranspiration rates at the 18 sites match with those obtained from the NLDAS-2 forcing dataset (NASA, 2021): when regressed against each other, R-squared values exceeded 0.95 for all locations. The derived soil moisture levels were compared against certified field observations and two alternative gridded products. Field data was obtained from NCEI's U.S. Climate Reference Network (NCEI, 2021), housing specialized soil moisture monitoring equipment. Seven USCRN sites were located within the analysis area, although comprehensive records before 2010 are unavailable. Therefore, 2011–2020 algorithm-derived soil moisture estimates were regressed against the observed values, using available daily climate parameters as an input into the algorithm. Missing values were again supplemented by the nearest GHCN or GSOD station. Hourly precipitation that exceeded the documented USCRN K_{sat} values for the seven locations were subtracted from daily totals, resulting in curtailed precipitation absorption. The two righthand columns of Table 4 display R-squared values from the algorithm regressed against the USCRN observations, with the rightmost column accounting for the new approach and showing a slight improvement in capturing real-world conditions.

To determine if the R-squared values represented an acceptable degree of accuracy and an improvement over existing soil moisture profile estimations, gridded soil moisture data from the Climate Forecast System Reanalysis (CFSR) (Saha *et al*., 2010) and the Global Land Data Assimilation System (GLDAS) (Rodell *et al*., 2004) were also obtained at the seven USCRN locations and regressed against historical data. By comparing columns 2 and 3 of Table 4 with the righthand columns, it is evident that the algorithm performed better than the prepackaged datasets when estimating location-specific moisture levels. The resolution of the sets – 0.20 deg. × 0.20 deg. (19 km) for the CFSR and 0.25 deg. × 0.25 deg. (24 km) for the GLDAS – contained homogenized values for areas with highly variable soil porosities, leading to discrepancies when compared to singular locations. Moreover, gridded products are known to contain biases that can differ based on proximity to the coastline etc. (Garibay *et al*., 2021; Huang *et al*., 2017). The USCRN validation showed the techniques deployed in this analysis, created for their ability to measure the evolving impacts of extreme precipitation runoff, were able to estimate soil moisture with improved modeling accuracy. One reason why R-squared values in the comparison validation were not closer to one was that daily USCRN soil data were calculated from hourly

Table 4. R-squared values of 2011-2020 parameter-derived soil moisture estimates, relative to USCRN soil observations (USCRN stations are also shown East to West).

USCRN Stn. (Lat./Lng.)	USCRN~CFSR R-squared	USCRN~GLDAS R-squared	USCRN~FAO-56* R-squared	USCRN~Adj. FAO-56* R-squared
Fairhp. (30.54, -87.87)	0.44***	0.40	0.69	0.70
Newton (32.33, -89.07)	0.53	0.51	0.88	0.89
Lafytt. (30.09, -91.87)	0.62	0.52	0.80	0.80
Palstn. (31.77, -95.72)	0.69	0.62	0.59	0.59**
Ednbrg. (26.52, -98.06)	0.54	0.42	0.72	0.73
Austin (30.62, -98.08)	0.69	0.57	0.72	0.74
Bronte (32.04, -100.24)	0.58	0.50	0.66	0.67

(*signifies the methodology deployed in this analysis, with the righthand column representing adjusted soil moisture estimates accounting for hourly precipitation rates)

(**sandy soils at this location have a K_{sat} value that exceeded all 2011-2020 precipitation rates)

(***the gridded CFSR product did not cover the immediate Mobile Bay shoreline, and so the regression was run using values 10 km East of the USCRN measurement location)

records. Therefore, a late-day soaking rain event was averaged with earlier dry conditions whereas the soil moisture algorithm calculated its water deficits at the end of the day, after all measurable precipitation had fallen.

4.4 Concluding Remarks

By developing easily reproducible techniques using certified climate parameter data, this study quantified the role of extreme precipitation in the development of drought in the U.S. South. Fueled by rising temperatures and vapor pressure deficits, higher reference evapotranspiration rates led to drier conditions in the study area, although the confidence level of deepening drought was less than that of ET_0. This caused increases in modeled irrigation water usage at 15 of 18 study area stations for the assumed grass surface covering to be maintained in a well-watered state. A station's climatology did not appear to be correlated with its aridification trend, as eastern humid and western semi-arid areas both housed stations with mixed trends of varying magnitude.

The well-established relationship between higher temperatures and the increased frequency and magnitude of extreme precipitation events has been documented over recent decades and is projected to accelerate with future anthropogenic warming. Estimating resulting impacts is essential when projecting future water demand for agricultural and municipal usage. The methodology introduced in the preceding study offers an alternative to gridded datasets and achieves better location-specific accuracy. It found accelerating aridity trends in 13 of the 15 highly-infiltrative soils that showed a change compared to the baseline. The approach is applicable to any region, although it is feasible at sites for which comprehensive climatological records are available.

Acknowledgments

Der-Chen Chang's research is partially supported by a National Science Foundation grant (DMS-1408839) and the McDevitt Endowment Fund at Georgetown University.

References

Al-Kaisi M, 2012: Pay Attention to Soil Crusting After Heavy Rain Events. https://crops.extension.iastate.edu/cropnews/2012/04. Accessed 12 April 2021.

Berg A, Famigliette J, Walker J *et al*., 2003: Impact of bias correction to reanalysis products on simulations of North American soil moisture and hydrological fluxes. *Journal of Geophysical Research Atmospheres* **108**, ACL 2-1 - ACL 2-15.

Bhatia N., Singh V, Lee K, 2019: Variability of extreme precipitation over Texas and its relation with climatic cycles. *Theoretical and Applied Climatology* **138**, 449–467.

Bishop D, Williams A, Seager R *et al*., 2018: Investing the Causes of Increased Twentieth-Century Fall Precipitation over the Southeastern United States. *Journal of Climate* **32**, 575–590.

Brown V, Keim B, Black A, 2019: Climatology and Trends in Hourly Precipitation for the Southeast United States. *Journal of Hydrometeorology* **20**, 1737–1755.

Brown V, Keim B, Black A, 2020: Trend Analysis of Multiple Extreme Hourly Precipitation Time Series in the Southeastern United States. *Journal of Applied Meteorology and Climatology* **59**, 427–442.

Clark J, Iverson L, Woodall C *et al*., 2016: The impacts of increasing drought on forest dynamics, structure, and biodiversity in the United States. *Global Change Biology* **22**, 2329–2352.

Easterling D, Kunkel K, Arnold J *et al*., 2017: Precipitation change in the United States. In *Climate Science Special Report: Fourth National Climate Assessment, Volume I*. [Wuebbles D, Fahey D, Hibbard K, Dokken D, Stewart B, Maycock T (eds.)]. U.S. Global Change Research Program, Washington, DC, USA, 207–230. doi:10.7930/J0H993CC.

Ferreira R, Nissenbaum M, Rickenbach T, 2018: Climate change effects on summertime precipitation organization in the Southeast United States. *Atmospheric Research* **214**, 348–363.

Ficklin D, Maxwell J, Letsinger S *et al*., 2015: A Climate deconstruction of recent drought trends in the United States. *Environmental Research Letters* **10**, 044009.

Garibay V, Gitau M, Kiggundu N *et al*., 2021: Evaluation of Reanalysis Precipitation Data and Potential Bias Correction Methods for Use in Data-Scarce Areas. *Water Resources Management* **35**, 1587–1602.

Guijarro J, 2019: Package *Climatol.* https://cran.rproject.org/web/packages/climatol/climatol.pdf. Accessed 18 October 2020.

Horton R,Yohe G, Easterling W *et al*., 2014: Ch. 16: Northeast. In *Climate Change Impacts in the United States: Third National Climate Assessment.* [Melillo J, Richmond T, Yohe G (eds.)] U.S. Global Change Research Program, Washington, DC, 371–395.

Howard J, Liang S, 2019: *U.S. Timber Production, Trade, Consumption, and Price Statistics*. U.S. Forest Service, Forest Products Laboratory, Madison, WI, 96 pp.

Huang H, Winter J, Osterberg E *et al*., 2017: Total and Extreme Precipitation Changes over the Northeastern United States. *Journal of Hydrometeorology* **18**, 1783–1798.

Janssen E, Wuebbles D, Kunkel K *et al*., 2014: Observational and model-based trends and projections of extreme precipitation over the contiguous United States. *Earth's Future* **2**, 99–113.

Jensen M, Allen R, 2016: *Evaporation, Evapotranspiration, and Irrigation Water Requirements*. 2nd ed. ASCE, https://ascelibrary.org/doi/book/10.1061/9780784414057.

Kharin V, Zwiers F, Zhang X *et al*., 2007: Changes in Temperature and Precipitation Extremes in the IPCC Ensemble of Global Coupled Model Simulations. *Journal of Climate* **20**, 1419–1444.

Kramer R, Bounoua L, Zhang P *et al*., 2015: Evapotranspiration Trends Over the Eastern United States During the 20th Century. *Hydrology* **2**, 93–111.

Lackmann G, 2013: The South-Central U.S. Flood of May 2010: Present and Future. *Journal of Climate* **26**, 4688–4709.

Lecce S, 2000: Spatial variations in the timing of annual floods in the southeastern United States. *Journal of Hydrology* **235**, 151–169.

Li L, Li W, Deng Y, 2013: Summer rainfall variability over the southeastern United States and its intensification in the 21st century as assessed by CMIP5 models. *Journal of Geophysical Research: Atmospheres* **118**, 340–354.

Liu C, Ikeda K, Rasmussen R *et al*., 2017: Continental-scale convection-permitting modeling of the current and future climate of North America. *Climate Dynamics* **49**, 71–95.

McGregor K, 2015: Comparison of the Recent Drought in Texas to the Drought of Record Using Reanalysis Modeling. *Papers in Applied Geography* **1**, 34–42.

Melillo J, Richmond T, Yohe G, Eds., 2014: *Climate Change Impacts in the United States: The Third National Climate Assessment*. U.S. Global Change Research Program, Washington, D.C. USA, 841 pp. doi:10.7930/J0Z31WJ2.

Mesinger F, DiMego G, Kalnay E *et al*., 2006: North American Regional Reanalysis. *Bulletin of the American Meteorological Society* **87**, 343–360.

Mishra V, Wallace J, Lettenmaier D, 2012: Relationship between hourly extreme precipitation and local air temperature in the United States. *Geophysical Research Letters* **39**, L16403.

National Aeronautics and Space Administration (NASA), 2021: NLDAS-2 Forcing Dataset Information. https://ldas.gsfc.nasa.gov/index.php/nldas/v2/forcing. Accessed 15 October 2021.

National Centers for Environmental Information (NCEI), 2021: U.S. Climate Reference Network. https://www.ncei.noaa.gov/access/crn. Accessed 10 October 2021.

National Oceanic and Atmospheric Administration (NOAA), 2012: 1981–2010 U.S. Climate Normals. https://www.ncdc.noaa.gov/data-access/land-based-station-data/land-based-datasets/climate-normals/1981-2010-normals-data. Accessed 23 February 2021.

National Weather Service, Climate Prediction Center, 2021: Soil Moisture Climatology. https://www.cpc.ncep.noaa.gov/products/Soilmst_Monitoring/US/Soilmst/Soilmst_clim.shtml. Accessed 10 March 2021.

Nearing M, Liu B, Risse L *et al*., 1996: Curve Numbers and Green-Ampt Effective Hydraulic Conductivities. *Water Resources Bulletin* **32**, 125–136.

Nielsen-Gammon J, Escobedo J, Ott C *et al*., 2020: *Assessment of Historic and Future Trends of Extreme Weather in Texas, 1900–2036.* Texas A&M University, Office of the Texas State Climatologist, College Station, TX, USA, 40 pp.

North Carolina Institute for Climate Studies, 2020: Portfolio: NEXRAD Radar Precipitation Reanalysis. https://ncics.org/portfolio/observing-systems/nexrad-radar-precipitation-reanalysis. Accessed 10 March 2021.

Rappaport E, Franklin J, Schumacher A *et al*., 2010: Tropical Cyclone Intensity Change before U.S. Gulf Coast Landfall. *Weather Forecast* **25**, 1380–1396.

Rasmussen K, Prein A, Rasmussen R *et al*., 2017: Changes in the convective population and thermodynamic environments in convection-permitting regional climate simulations over the United States. *Climate Dynamics* **55**, 383–408.

Rawls W, Ahuja L, Brakensiek D *et al*., 1993: Infiltration and Soil Water Movement. In *Handbook of Hydrology* [Maidment, D (ed.)]. McGraw-Hill, Inc., New York, NY, USA. ISBN: 0070397325.

Rodell M, Houser P, Jambor U *et al*., 2004: The Global Land Data Assimilation System. *Bulletin of the American Meteorological Society* **85**, 381–394.

Saha S, Moorthi S, Pan H *et al*., 2010: The NCEP Climate Forecast System Reanalysis. *Bulletin of the American Meteorological Society* **91**, 1015–1057.

Seager R, Lis N, Feldman J *et al*., 2018: Whither the 100th Meridian? The Once and Future Physical and Human Geography of America's Arid-Humid Divide. Part I: The Story So Far. *Earth Interactions* **22**, 1–22.

Skeeter W, Senkbeil J, Keellings D, 2019: Spatial and temporal changes in the frequency and magnitude of intense precipitation in the southeastern United States. *International Journal of Climatology* **39**, 768–782.

Smith R, Chang D, 2020: Utilizing Recent Climate Data in Eastern Texas to Calculate Trends in Measures of Aridity and Estimate Changes in Watering Demand for Landscape Preservation. *Journal of Applied Meteorology and Climatology* **59**, 143–152.

Smith R, Guijarro J, Chang D, 2020: Utilizing homogenized observation records and reconstructed time series data to estimate recent trends in Mid-Atlantic soil moisture scarcity. *Theoretical and Applied Climatology* **143**, 1063–1076.

Texas Water Development Board, 2017: *State Water Plan*. State of Texas, Austin, TX, USA, 134 pp.

Trenberth K, 2011: Changes in precipitation with climate change. *Climate Research* **47**, 123–138.

Trenberth K, Zhang Y, Gehne M, 2017: Intermittency in precipitation: Duration, frequency, intensity, and amounts using hourly data. *Journal of Hydrometeorology* **18**, 1393–1412.

United States Department of Agriculture, Economic Research Service, 2017: Major Land Uses. https://www.ers.usda.gov/data-products/major-land-uses. Accessed 23 February 2021.

United States Department of Agriculture, National Resources Conservation Service, 2019: Web Soil Survey. https://websoilsurvey.sc.egov.usda.gov. Accessed 25 February 2021.

United States Department of Agriculture, Natural Resources Conservation Service, 1999: *Soil Taxonomy: A Basic System of Soil Classification for Making and Interpreting Soil Surveys.* U.S. Government Printing Office, 886 pp.

United States Department of Agriculture, National Resources Conservation Service, 2003: Soil Survey Technical Note 6: Saturated Hydraulic Conductivity: Water Movement Concepts and Class History. Accessed 1 April 2020.

Wang S, Zhao L, Yoon J, *et al*., 2018: Quantitative attribution of climate effects on Hurricane Harvey's extreme rainfall in Texas. *Environmental Research Letters* **13**, 054014.

Wehner M, Arnold J, Knutson T *et al*., 2017: Droughts, floods, and wildfires. In *Climate Science Special Report: Fourth National Climate Assessment, Volume I.* [Wuebbles D, Fahey D, Hibbard K, Dokken D, Stewart B *et al*. (eds.)]. U.S. Global Change Research Program, Washington, DC, USA 231–256. doi:10.7930/J0CJ8BNN.

Wright J, 1993: Nongrowing season ET from irrigated fields. [Allen R, Neale C (eds.)]. *Management of Irrigation and Drainage Systems: Integrated Perspectives*, ASCE Irrigation and Drainage Division, Park City, UT, USA, 1005–1014.

Zhang W, Villarini G, Vecchi G *et al*., 2018: Urbanization exacerbated the rainfall and flooding caused by hurricane Harvey in Houston. *Nature* **563**, 384–388.

Zhu Z, Piao S, Zeng N, 2016: Greening of the Earth and its drivers. *Nature Climate Change* **6**, 791–795.

Zontarelli L, Dukes M, Romero *et al*., 2010: Step by step calculation of the Penman-Monteith evapotranspiration (FAO-56 method). University of Florida Institute of Food and Agricultural Sciences Doc. AE459, 10 pp., https://edis.ifas.ufl.edu/ae459. Accessed 2 February 2020.